Bayesian Inverse Modelling of Early-Age Stress Evolution in GGBFS Concrete Due to Autogenous Deformation and Aging Creep

Minfei Liang(✉), Erik Schlangen, and Branko Šavija

Microlab, Faculty of Civil Engineering and Geosciences, Delft University of Technology, 2628 Delft, The Netherlands
{M.Liang-1,Erik.Schlangen,B.Savija}@tudelft.nl

Abstract. Stress evolution of restrained concrete is directly related to early-age cracking (EAC) potential of concrete, which is a tricky problem that often happens in engineering practice. Due to the global objective of carbon reduction, Ground granulated blast furnace slag (GGBFS) concrete has become a more promising binder comparing with Ordinary Port-land Cement (OPC). Although GGBFS concrete produces less hydration heat which further prevents thermal shrinkage, the addition of GGBFS highly increases the autogenous shrinkage and thus increases EAC risk. This study presents experiments and numerical modelling of the early-age stress evolution of GGBFS concrete, considering the development of autogenous deformation and creep. Temperature Stress Testing Machine (TSTM) tests were conducted to obtain the autogenous deformation and stress evolution of restrained GGBFS concrete. By a self-defined material sub-routine based on the Rate-type creep law, the FEM model for simulating the stress evolution in TSTM tests was established. By characterizing the creep compliance function with a 13-units continuous Kelvin chain, forward modelling was firstly conducted to predict the stress development. Then inverse modelling was conducted by Bayesian Optimization to efficiently modify the arbitrary assumption of the codes on the aging creep. The major findings of this study are as follows: 1) the high autogenous expansion of GGBFS induces compressive stress at first hours, but its value is low because of high relaxation and low elastic modulus; 2) The codes highly underestimated the early-age creep of GGBFS concrete. They performed well in prediction of stress after 200 h, but showed significant gaps in predictions of early-age stress evolution; 3) The proposed inverse modelling method with Bayesian Optimization can efficiently adjust the aging terms which produced best modelling results. The adjusted creep compliance function of GGBFS showed a much faster aging speed at early ages than the one proposed by original codes.

Keywords: Concrete · Bayesian Optimization · Early age cracking · Creep · Relaxation · Autogenous shrinkage

1 Introduction

Early-age cracking (EAC) is one of the trickiest problems happened to early-age concrete structures. The hydration-induced volume shrinkage (i.e., autogenous shrinkage) and

P. Rossi and J.-L. Tailhan (Eds.): SSCS 2022, RILEM Bookseries 38, pp. 207–217, 2023.
https://doi.org/10.1007/978-3-031-07746-3_21

external restraint result in accumulation of tensile stress, which may exceed the tensile strength of concrete and cause EAC. During this process, the evolution of elastic modulus, shrinkage, creep and environmental conditions (e.g., temperature) together determines the buildup of tensile stress.

Ground granulated blast furnace slag (GGBFS) has been used as a popular supplementary cementitious material (SCMs), which can highly decrease the hydration heat but increase autogenous shrinkage [1, 2]. Thereby, for EAC analysis of GGBFS concrete, the autogenous shrinkage appears to be a more influential factor than thermal shrinkage. Another factor that strongly influences the EAC risk is the early-age creep/relaxation, which directly influences the accumulation of tensile stress and therefore should not be neglected in all cases of EAC analysis [3]. Comparing to elastic modulus, early-age creep is much more difficult to measure, as the effects of hydration process and creep/relaxation cannot be fully decoupled, especially in early-age. A potential solution is minutes-repeated short-term creep test, because the hydration effects can be neglected in such a short-term [4]. However, minutes-long short-term creep tests are not likely to fully reflect the creep behaviour of concrete in a longer time-range. EAC analysis requires the input of creep compliance function $J\ (t, t')$ (or relaxation modulus $R\ (t, t')$) that is continuous at time of loading t' and longing duration t.

To evaluate the EAC risk, a number of restraint tests have been performed, such as rigid cracking frame test, internal restraint test, ring test, and temperature-stress testing machine test (TSTM) [5–9]. Among these tests, TSTM stands out due to its advantages of tunable temperature control, loading scheme and restraint degree. In this paper, we aim to establish a modelling framework for early-age stress evolution due to autogenous shrinkage and aging creep. Based on Rate-Type Creep Law and exponential algorithm, the creep/relaxation of early-age concrete is quantified by a 13-Unit Kelvin Chain. Then, based on Bayesian Optimization and stress results of TSTM tests, the aging creep is quantified efficiently within the framework of EURO code and ACI code.

2 Methods

The stress evolution of restrained concrete is the basic and direct index for evaluating the EAC risk. Based on Boltzmann superposition, the stress evolution initiated from different time of loading t_0 by shrinkage and creep is quantified. However, integrating the whole stress history poses to be a computational dilemma because it requires to save all stress results at every step and FEM elements. Thereby, this paper incorporates the Rate-type Creep Law, which avoids the complex stress integration and only needs to solve an incremental quasi-elastic constitutive equation at every step [10, 11]. Furthermore, in view of the unattainable experimental input for aging creep, this paper conducts Bayesian Optimization to achieve fast and efficient inverse modelling for the continuous creep compliance function $J\ (t, t')$.

2.1 Viscoelastic Material Subroutine

Based on the Boltzmann superposition, the creep strain can be expressed by the following integration:

$$\varepsilon(t) = \int_0^t J\left(t, t'\right) \mathrm{d}\sigma\left(t'\right) \tag{1}$$

where J is the creep compliance function. Writing Eq. (1) in an incremental form and approximate a linear stress variation in each time interval, one gets the aforementioned quasi-elastic constitutive equation that needs to be solved at every time step:

$$\Delta\sigma = E^*\Delta\varepsilon - \sigma^* \tag{2a}$$

$$E^* = \frac{\Delta t}{\int_{t_i}^{t_{i+1}} J(t_{i+1}, t')dt'} \tag{2b}$$

$$\sigma^* = E^* \int_0^{t_i} \left[J\left(t_{i+1}, t'\right) - J\left(t_i, t'\right)\right]\dot{\sigma}\, dt' \tag{2c}$$

where $\Delta\sigma$ and $\Delta\varepsilon$ are difference of stress and strain between two consecutive time steps t_i and t_{i+1}. The creep compliance curve can be expressed as a Dirichlet series, which can be the governing equations of Kelvin chain rheological model with sets of spring and dashpot:

$$J\left(t, t'\right) = \frac{1}{E_0(t')} + \sum_{j=1}^{N} \frac{1}{E_j(t')}\left(1 - e^{-\frac{t-t'}{\mu_j}}\right) \tag{3}$$

where N is the number of Kelvin chain units; E_j and μ_j is the elastic modulus and retardation time of j-th Kelvin chain units. Substituting Eq. (3) in Eq. (2) and calculate the integral by mid-point rule, one can obtain the E^* and σ^* in Eq. (2) as follows [10, 11]:

$$E^*\left(t^*\right) = \frac{1}{\frac{1}{E_0(t^*)} + \sum_{j=1}^{N} \frac{1}{E_j(t^*)}\left(1 - \left(1 - e^{-\frac{\Delta t}{\mu_j}}\right)\frac{\mu_j}{\Delta t}\right)} \tag{4a}$$

$$\sigma^*(t_i) = E^*\left(t^*\right) \sum_{j=1}^{N} \left(1 - e^{-\frac{\Delta t}{\mu_j}}\right)\varepsilon_j^*(t_i) \tag{4b}$$

$$\varepsilon_j^*(t_i) = \int_0^{t_i} \frac{1}{E_j(t')} e^{-\frac{t_i - t'}{\mu_j}}\dot{\sigma}\, dt' \tag{4c}$$

$$\varepsilon_j^*(t_{i+1}) = e^{-\frac{\Delta t}{\mu_j}}\varepsilon_j^*(t_i) + \frac{1}{E^*(t_i)}\left(1 - e^{-\frac{\Delta t}{\mu_j}}\right)\frac{\mu_j}{\Delta t}\Delta\sigma \tag{4d}$$

where t* is the average of two consecutive time steps t_i and t_{i+1}. Equation (2a) and Eq. (4) form the incremental quasi-elastic constitutive equation of this paper.

2.2 FEM Configuration

Incorporating the influence of autogenous shrinkage, the aforementioned quasi-elastic constitutive equation Eq. (2a) becomes:

$$\Delta\sigma = E^*(\Delta\varepsilon - \Delta\varepsilon_{ad}) - \sigma^* \tag{5}$$

where $\Delta\varepsilon_{ad}$ is the autogenous strain happening in each time interval. As shown in Eqs. (4) and (5), there are mainly 3 input parameters: 1) Elastic modulus, 2) autogenous shrinkage and 3) Creep compliance curve characterized by Kelvin chain parameters. The elastic modulus is computed by the empirical formulas of Model Code 2010 [12] based on the compressive strength test, and the autogenous shrinkage is directly extracted from ADTM tests, which are presented in our dual paper submitted to this conference and previous works [13, 14]. The creep compliance formula of ACI and EURO codes are tentatively used as input of this paper [15, 16]. Their creep compliance formula can be expressed as:

$$J(t,t') = \frac{1}{E(t')} + C_0C_1(t')C_2(\xi) \tag{6}$$

where C_0 is a coefficient related to general concrete properties and environmental conditions; C_1 is a power function to describe the aging of creep compliance; C_2 is a power function representing the non-aging term, which mainly depends on the time length of loading ξ ($\xi = t-t'$). To fit the Eq. (10) into a Dirichlet series as in Eq. (3), the procedure proposed by Bazant is adopted, which guarantees a unique and stable solution when fitting a continuous spectrum of Kelvin chain parameters [17–19]. Firstly, the retardation time μ_j is chosen as a priori to prevent ill-conditioned equation system as follows:

$$\mu_j = 10^{-6+j},\ j = 1:13 \tag{7}$$

The continuous form of the non-aging term is expressed as follows:

$$C_2(\xi) = \int_0^\infty \frac{1}{E_j}\left(1 - e^{-\frac{\xi}{\mu_j}}\right)\mathrm{d}(ln\mu_j) \tag{8}$$

Using the Laplace transform and Widder's formula, the solutions of E_j can be derived as:

$$\frac{1}{E_j} = -ln10 * \lim_{k\to\infty} \frac{(-k\mu)^k}{(k-1)!}C_2^{(k)}(k\mu) \tag{9}$$

In this paper, the spectrum of third order (k = 3) is used. The fitting results of the mixes with w/c = 0.35 based on EURO code is shown as an example in Fig. 1, which shows that the fitted Kelvin chain can mimic the codes with good precision.

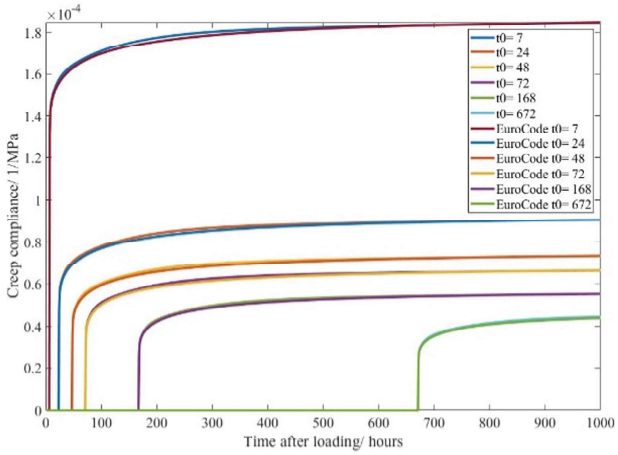

Fig. 1. Fitting results of Kelvin chain with codes (Euro Code w/c = 0.35)

Having set up the constitutive equation and input parameters, the TSTM tests can be simulated properly. The dog-bone specimen used in TSTM, and corresponding mesh and boundary settings are shown in Fig. 2. Roller boundaries are attached to the highlighted purple area in Fig. 2(b) (i.e., bottom sides and the lateral sides of the two ends), which ensues zero displacement in the normal direction of the boundary surface.

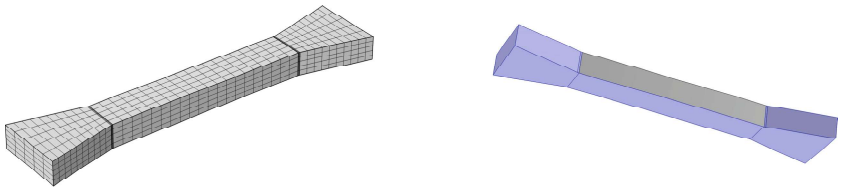

(a) mesh (b) boundary conditions

Fig. 2. Numerical dog-bone specimen

The modelling result of stress evolution σ_M is calculated at the middle section of the specimen and expressed as follows:

$$\sigma_M(t) = \frac{\iint \sigma_{xx} dydz}{A} \tag{10}$$

where σ_{xx} is the component of stress tensor in xx direction (i.e., axial direction of dog-bone specimen); A is the cross-section area. The metric Root Mean Squared Error (RMSE) is adopted to quantify the modelling accuracy by averaging the residual error at each time step:

$$RMSE = \sqrt{\frac{\sum_t (\sigma_M(t) - \sigma_T(t))^2}{t_{total}}} \tag{11}$$

where $\sigma_M(t)$ and $\sigma_T(t)$ is modelling and testing results of stress at time step t.

2.3 Bayesian Inverse Modelling

To cope with the testing dilemma of aging creep tests, this study implements Bayesian Inverse Modelling to derive a continuous aging creep compliance surface. Based on Sects. 2.1 and 2.2, the following black-box function can be obtained:

$$RMSE = f\left[\varepsilon_{ad}(t), E(t), J\left(t, t'\right), \sigma_T(t)\right] \tag{12}$$

Then the inverse modelling process can be defined as the following optimization process:

$$\arg\min f\left\{J\left(t, t'\right) | \varepsilon_{ad}(t), E(t), \sigma_T(t)\right\} \tag{13}$$

Recalling the creep compliance formulas given by the codes in Eq. (7), one can find that the constant term C_0 and non-aging term C_2 both depends on specific mi parameters and environmental conditions, while the aging term C_1 remains unchanged for any mixes and environmental conditions. The codes cannot reflect the difference of aging creep of different mixes [20, 21]. Thereby, the inverse modelling process focuses on the aging term C_1, which can be formulated as follows for both codes:

$$\text{Euro code}: \; C_1\left(t'\right) = \frac{c}{b + t'^a}; \tag{14a}$$

$$\text{ACI code}: \; C_1\left(t'\right) = \frac{c}{t'^a} \tag{14b}$$

where a, b, and c are fitting parameters. The inverse modelling process can then be described as follows:

$$\arg\min f\left\{C_1\left(t', a, b, c\right) | \varepsilon_{ad}(t), E(t), \sigma_T(t), C_0, C_2\left(t - t'\right)\right\} \tag{15}$$

Implementing the optimization process described by Eq. (15), one has to reiterate the FEM model described in Eq. (12) to find the lowest RMSE optima. This process can be inefficient when coping with complex FEM models which requires considerable amount of time to run. Thereby, we propose to implement Bayesian Optimization to achieve fast solution of Eq. (15). Bayesian Optimization is composed by two major parts: a Gaussian Process predictor and an acquisition function [22, 23], as shown in Fig. 3.

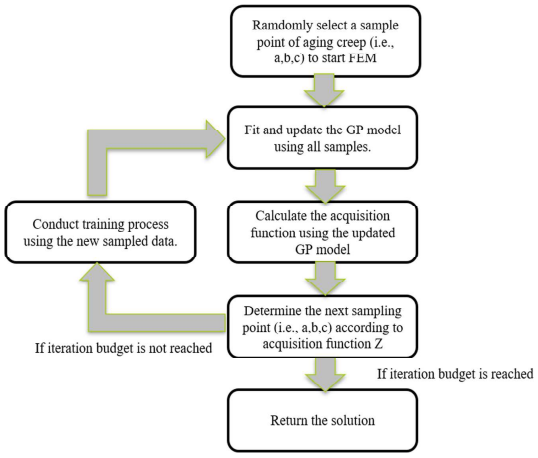

Fig. 3. Workflow of Bayesian optimization

Assuming the sampling points X *(a,b,c)* and corresponding *RMSE* of each FEM trial follows the multivariate Gaussian distribution, denoted as $D_{1:n} = (X_{1:n}, Y_{1:n})$, the Bayesian inference of next sampling points can be expressed as:

$$Y_{n+1}|\mathrm{D}_{1:n} \sim \mathrm{N}\left(\mu(\mathrm{X}_{n+1}), \sigma^2(\mathrm{X}_{n+1}) + \sigma^2_{noise}\right) \tag{16}$$

in which

$$\mu(\mathrm{X}_{n+1}) = \boldsymbol{k}^T K^{-1} Y_{1:n} \tag{17a}$$

$$\sigma^2(\mathrm{X}_{n+1}) = k(\mathrm{X}_{n+1}, \mathrm{X}_{n+1}) - \boldsymbol{k}^T \left(K + \sigma^2_{noise}\boldsymbol{I}\right)^{-1} \boldsymbol{k} \tag{17b}$$

$$\boldsymbol{k} = \left[k(X_{n+1}, X_1) k(X_{n+1}, X_2) \cdots k(X_{n+1}, X_n)\right] \tag{17c}$$

$$K = \begin{bmatrix} k(X_1, X_1) & \cdots & k(X_1, X_n) \\ \vdots & \ddots & \vdots \\ k(X_n, X_1) & \cdots & k(X_n, X_n) \end{bmatrix} + \sigma^2_{noise}\boldsymbol{I} \tag{17d}$$

where k is the covariance kernel between any two sampling points X_i and X_j, calculated by an exponential function of the second norm of the difference value between two samples; $\boldsymbol{k}$ is a n-by-1 covariance matrix of the new sampling point X_{n+1} and n sampling points $X_1 \sim X_n$; K is the n-by-n covariance matrix of any two sampling points assembled by k. With the GP predictor (Eqs. 16 and 17), the inference of RMSE based on any combinations of (a,b,c) can be made. Then, the acquisition function Expected Improvement is adopted to infer the improving potential of every possible sample point, expressed as below:

$$I(X_n) = \left(\mathrm{y}_{best} - \mu(\mathrm{X}_n)\right)\Phi\left(\frac{\mathrm{y}_{best} - \mu(\mathrm{X}_n)}{\sigma(\mathrm{X}_n)}\right) + \sigma(\mathrm{X}_n)\phi\left(\frac{\mathrm{y}_{best} - \mu(\mathrm{X}_n)}{\sigma(\mathrm{X}_n)}\right) \tag{18}$$

where $\Phi(\cdot)$ and $\phi(\cdot)$ are the standard normal density and distribution function; y_{best} is the tentative optimal value (i.e., lowest RMSE) in current sample space. At evert iteration, the sampling point with the highest I will be chosen to run the next FEM simulation.

3 Results and Discussion

In this section, the modelling results of the testing results of w/c = 0.35 in our dual paper [13] will be presented.

3.1 Forward Modelling with Codes

The modelling results directly using the creep formulas of codes are shown in Fig. 4. An obvious gap between the code results and tests can be seen at very early-age, approximately before 150 h, which indicates that the codes' assumptions of the constant aging pattern for concrete creep are not applicable, as expected. However, after 150 h, the curves of modelling stress tend to be more parallel with the testing results, which indicates that both codes show good conformity with TSTM testing results at a latter age. Therefore, most modelling error lie in the early-age creep inference made by codes. If the time-zero of the models and tests are fixed at a time point after 150 h, good conformity between the modelling and testing results can be expected. But in the meantime, this will also cause significant errors since the stress before 200 h is overlooked.

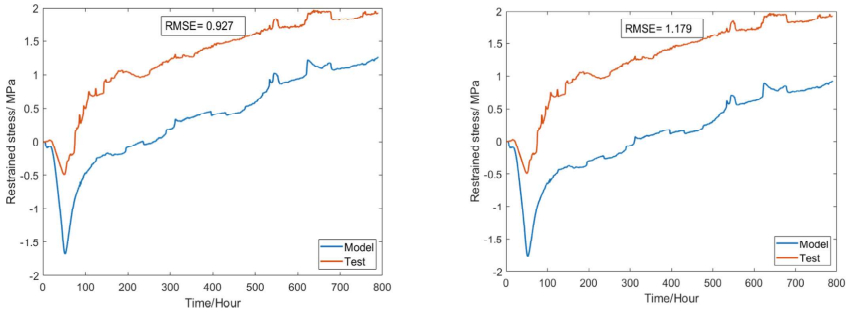

(a) model with ACI creep (b) model with EURO creep

Fig. 4. Simulated stress evolution with different codes for creep compliance

3.2 Inverse Modelling with Adjusted Codes

Following the procedure described in Sect. 2.3, the adjusted terms for aging creep can be obtained. The optimization history is shown in Fig. 5. The optimization history shows a fast convergence of this method, within around 5 steps for ACI and 12 steps for EURO code. The reason why EURO code needs more computation budget is that its aging term has 3 parameters, while the ACI only has 2. Figure 5(b) shows that the sampling points tends to be much denser when approaching to the minima, and more diluted

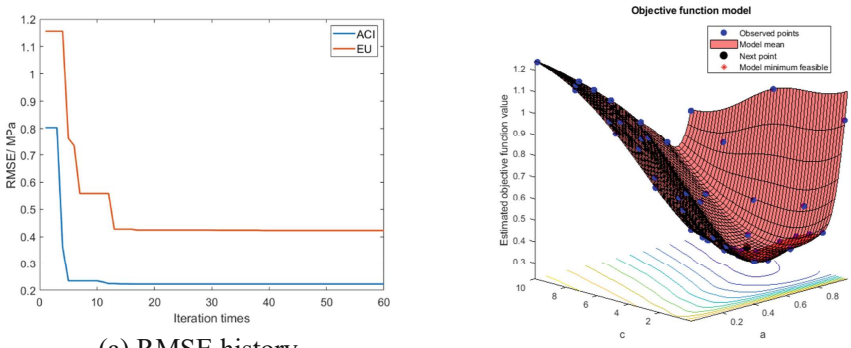

(a) RMSE history (b) Response surface

Fig. 5. Optimization history

when approaching to the peaks, which guarantees the tradeoff between exploitation and exploration and therefore ensure the efficiency.

Accordingly, the modelling results with the adjusted aging terms are shown in Fig. 6. The results show obvious improvement comparing with results based on codes. Most of the improvement is on early-age stress. However, the modelling results are still not perfect, this can be explained by the following potential reasons: 1) the experimental curves are not smooth due to friction and temperature fluctuation. With the objective goal defined in Eq. (15), the model has to make compromise at every time points of the experimental curves; 2) the aging function proposed by the codes are different and may not suitable to fully reflect the aging pattern of concrete creep. As shown in the results based on original codes, the aging term creates gaps between first 150 h, while works well on a time-range after 150 h. However, in the inverse modelling process, the changes on parameters (a, b, c) change the whole aging function, which means that although the improvement at first 150 h can be made, the good performance of original code after 150 h is also compromised. The final results based on the specific function forms are the tradeoff described above and therefore are not perfect.

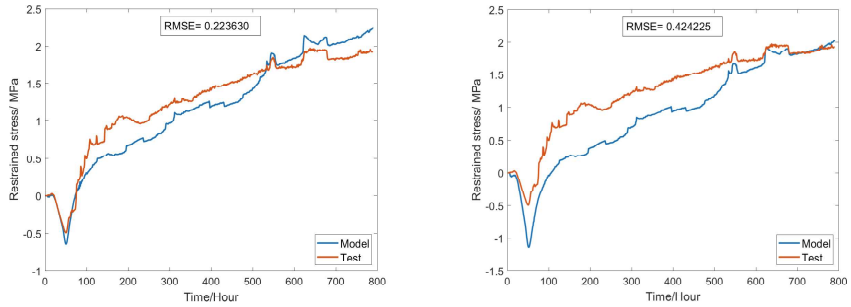

(a) model with ACI creep (b) model with EURO creep

Fig. 6. Modelling results with adjusted aging term of creep

4 Conclusion

1) The modelling results show that creep formulas proposed by ACI and EURO codes performs well in later ages (after 200 h in this paper), which in turn validated the proposed FEM model in modelling the stress evolution of restrained concrete.
2) Due to the arbitrary settings in the aging of creep, modelling results based on both codes show significant gap at early ages before 200 h.
3) Inverse modelling based on Bayesian Optimization can guarantee efficiently find the optimal aging terms of creep compliance formulas, which can then used to predict the stress development of restrained concrete with higher accuracy.

References

1. Tianshi, L., Li, Z., Huang, H.: Effect of supplementary materials on the autogenous shrinkage of cement paste. Materials **13**, 3367 (2020)
2. Darquennes, A., Khokhar, M.I.A., Rozière, E., Loukili, A., Grondin, F., Staquet, S.: Early age deformations of concrete with high content of mineral additions. Constr. Build. Mater. **25**, 1836–1847 (2011)
3. Azenha, M., Kanavaris, F., Schlicke, D., et al.: Recommendations of RILEM TC 287-CCS: thermo-chemomechanical modelling of massive concrete structures towards cracking risk assessment. Mater. Struct. **54**, 135 (2021)
4. Irfan-ul-Hassan, M., Pichler, B., Reihsner, R., Hellmich, C.: Elastic and creep properties of young cement paste, as determined from hourly repeated minute-long quasi-static tests. Cem. Concr. Res. **82**, 36–49 (2016)
5. Spingenschmid, R.: Prevention of Thermal Cracking in Concrete at Early Ages. E&FN Spon, London (1998)
6. Semianiuk, V., Tur, V., Herrador, M.F.: Early age strains and self-stresses of expansive concrete members under uniaxial restraint conditions. Constr. Build. Mater. **131**, 39–49 (2017)
7. Briffaut, M., Benboudjema, F., D'Aloia, L.: Effect of fibres on early age cracking of concrete tunnel lining. Part I: Laboratory ring test. Tunnel. Underground Space Technol. **59**, 215–220 (2016)
8. Shen, D., Jiang, J., Shen, J., Yao, P., Jiang, G.: Influence of curing temperature on autogenous shrinkage and cracking resistance of high-performance concrete at an early age. Constr. Build. Mater. **103**, 67–76 (2016)
9. Markandeya, A., Shanahan, N., Gunatilake, D.M., Riding, K.A., Zayed, A.: Influence of slag composition on cracking potential of Slag-Portland cement concrete. Constr. Build. Mater. **164**, 820–829 (2018)
10. Di Luzio, G., Cedolin, L., Beltrami, C.: Tridimensional long-term finite element analysis of reinforced concrete structures with rate-type creep approach. Appl. Sci. **10**, 4772 (2020)
11. Bažant, Z.P., Jirásek, M.: Creep and Hygrothermal Effects in Concrete Structures. Springer, Dordrecht (2018)
12. International Federation for Structural Concrete (fib), Fib Model Code for Concrete Structures 2010. Ernst & Sohn, Wiley, Berlin (2013)
13. Schlangen, E., Liang, M., Šavija, B.: The influence of autogenous shrinkage and creep on the risk of early age cracking. In: RILEM International Conference Numerical Modelling Strategies for Sustainable Concrete Structures, Marseille (2022)